ZIF-8, chitosan and β-cyclodextrin-incorporated ZIF-8 nanohybrid for improving drug delivery

Weenawan Somphon*, Arthorn Loisruangsin

Division of Chemistry, Department of Physical and Material Sciences, Faculty of Liberal Arts and Science, Kasetsart University Kamphaeng Saen Campus, Nakhon Pathom 73140 Thailand

*Corresponding author, e-mail: weenawan.s@ku.th

ABSTRACT: The success of encapsulation of two model drugs, anti-Alzheimer donepezil (DH) and antibiotic nitrofurantoin (NF), in ZIF-8 through the one-pot method was reported here. The one-pot method was further applied to incorporate chitosan (CS) or β-cyclodextrin (BCD) into the encapsulation of the drug in ZIF-8. The characterization of the samples was carried out experimentally *via* UV-vis spectroscopy, FT-IR, XRD, SEM, TEM, TGA, and zeta potential analysis; and computationally *via* molecular docking and geometric optimization calculations. The drug loadings and drug releases of the samples were then explained. The binding interaction of the model drugs on other components and morphology and molecular weight of the coating material affects both the drug loading and drug release. DH mainly contributed in the interior and on the surface of ZIF-8. Free voids of the coating CS were assumed to play the role of NF loading since the binding of NF to the surface of ZIF-8 was limited by the N-Zn coordinate bond. Physical properties of coating materials such as viscosity and solubility were considered for explaining different drugs at a neutral pH, while the protonation of the amine group of DH or CS became predominant for the drug release at an acidic pH.

KEYWORDS: zeolitic imidazolate frameworks, drug delivery, chitosan, cyclodextrin, donepezil

INTRODUCTION

Porous materials are combined to create a new category of drug delivery systems because they have stable structures with high surface areas and tunable pore sizes. They have been used to create drug delivery systems like sustained drug delivery and to improve the solubility of poorly soluble drugs [1]. Zeolitic Imidazolate Framework-8 (ZIF-8) is a popular drug delivery vehicle because of its good biocompatibility, high drug loading capacity, tunable functionality, and high thermal stability [2]. Under physiological conditions, ZIF-8 is very stable; but it decomposes quickly under acidic conditions, hence, we were interested in improving its biostability for drug application. There were some reports demonstrating the enhanced solubility of drugs by ZIF-8 NPs with polymer PAA@ZIF-8 NPs [3] and the enhancement of biocompatibility and degradability by the pH-sensitive ZIF-8 PDA-PCM@ZIF-8 [4].

Polysaccharides have been reported to have the ability to improve the therapeutics of drugs such as antibiotics by controlling target drug delivery [5]. For example, the hyaluronic acid-coated ZIF-8 nanocomposite enhanced drug delivery [6], and ZIF-8 combined with alginate protected the collapse of ZIF-8 in acidic environments and improved the biostability of the target drug at high pH [7]. Due to its biological properties of non-toxicity, biocompatibility, biodegradability, and mucoadhesive ability [5], chitosan (CS) is widely recognized as a promising drug carrier, such as chitosan-based nanoparticles [8]. Previous research [9] found that CS-coated MIL-100 (Fe) nanoparticles improved intestinal permeability by increasing colloidal stabil-

ity and biodegradation. Also, β-cyclodextrin (BCD) is an oligosaccharide with its structure containing a hydrophobic interior cavity and a hydrophilic exterior surface. The primary advantage of BCD was its ability to improve the solubility and stability of drug molecules [10, 11]. The Fe (III) trimester nanoparticle was coated with cyclodextrin [12], which improved colloidal stability in body fluids.

Chitosan-based nanoparticles had the potential to be used as a drug carrier for targeted brain delivery [15]. Besides, a previous study reported a sustained drug release by donepezil-loaded chitosan nanoparticle [16]. Furthermore, the formation of donepezil with cyclodextrin [17] enhanced donepezil solubility by improving the dynamic process and drug absorption, as well as the stability of the transition from the oral cavity to the stomach. Computational methods, such as molecular docking and density functional-based tight-binding (DFTB), assisted in investigating binding pair interactions of all components involving in one-pot synthesis.

In this study, we demonstrated the CS and BCD, as a hybrid polymer with ZIF-8 to improve drug delivery systems. Two drug models were encapsulated: the anti-drug Alzheimer's donepezil (DH) and the antibiotic nitrofurantoin (NF). The major disadvantages of these two drugs are their physicochemical stability and bioavailability [13, 14].

MATERIALS AND METHODS

Materials and characterization techniques

$Zn(NO_3)_2 \cdot 6H_2O$ (98%), donepezil hydrochloride

(98%), chitosan (∼160 kDa), and β-cyclodextrin (97%) were purchased from Sigma-Aldrich, Singapore. 2-Methylimidazole (97%) and nitrofurantoin (98%) were purchased from Alfa Aesar, Korea and ACROS Organics, Thailand, respectively.

UV-vis absorption spectra were recorded by a T80 UV-visible spectrophotometer (PG Instruments), and collected in the 200–800 nm range. The surface morphology was determined by using FE-SEM of JEOL, JMS-7600F at an accelerating voltage of 3 kV; and the TEM of JEOL, JEM-1230 operated at 120 kV. Image J was used to calculate the average particle size of the crystal. The FT-IR was measured by a Perkin Elmer Spectrum GX with a wavenumber in the range of 4000–500 cm^{-1} with an ATR detector and a diamond Zn/Se crystal accessory. XRD was performed using a Bruker Model, D8 Advance with Cu-Kα radiation at 40 kV, 30 mA, 2θ from 5 to 80° in steps of 0.02° and a scan speed of 0.05 s/step. Thermogravimetric analysis was performed with a NETZSCH/TG 209 F1 Libra in the range of 50–800 °C under N_2 gas at a heating rate of 10 °C/min in an alumina pan. The zeta potential was measured with the Master 3000 (Malvern Particle Instruments Ltd., UK). The measurement was recorded in DI water at 25 °C as a function of pH using 0.5 M NaOH and 0.5 M HCl.

Synthesis and characterization of ZIF-8, and drug-encapsulated in ZIF-8

This experiment used two drugs, DH and NF. The stock solutions (0.05% w/v) of each drug were prepared in PBS pH 7.4. ZIF-8 was synthesized using a modified version of the [18] procedure, in which 0.6 g $Zn(NO_3)_2 \cdot 6 H_2O$ was dissolved in 10 ml methanol; and 1.3 g 2-methylimidazole (2-MeIm) was dissolved in 10 ml methanol. The zinc nitrate solution was then dropped into the 2-MeIm solution and magnetically stirred for 1 h. The synthesized product was collected by centrifugation for 10 min and washed with methanol 5 times, and the solvent was removed by rotary evaporation for 1 h. The final product was dried in the oven at 100 °C for 12 h. Drugs were encapsulated in ZIF-8 by immersing 100 mg of ZIF-8 in 4 ml of the drug (2 mg) solutions and stirring for 24 h with a magnetic stirrer. Following all steps of the synthesis pathway, the crystalline products of NF-loaded ZIF-8 and DH-loaded ZIF-8 were obtained and evaluated by UV-vis spectroscopy, FT-IR, FE-SEM, XRD, and TGA.

One-pot synthesis of drug@ZIF-8, drug@ZIF-8/CS and drug@ZIF-8/BCD

One pot each of DH@ZIF-8 and NF@ZIF-8 was prepared by dissolving 150 mg of $Zn(NO_3)_2 \cdot 6 H_2O$ in 5 ml of DI water. Then, the drug solution (2 mg in 4 ml of PBS) was added to the zinc nitrate solution and magnetically stirred. After that, 330 mg of 2-MeIm

was dropped into the solution and magnetically stirred for 30 min. Finally, the product was centrifuged for 10 min and washed with methanol 5 times; the solvent was removed by rotary evaporation for 1 h and dried at room temperature under vacuum.

Separately, 100 mg of ZIF-8 and 10 mg of CS in 4 ml of 1% acetic acid; or 100 mg of BCD, was added to 4 ml each of the 0.05% w/v anti-drug DH and the antibiotic NF. The two mixtures were magnetically stirred for 24 h, and the precipitates were separated following the same steps of the one-pot synthesis of ZIF-8.

Drug loading and release studies

UV-vis spectroscopy was used to determine the amount of drug-loaded materials. Five mg of free drug and drug-loaded materials were dissolved in 10 ml PBS pH 7.4 and decomposed with 1 drop (50 µl) of 1 M HCl at 37 °C for 72 h before being collected by centrifugation for 10 min. The centrifuged solution was filtered through a nylon filter and then examined by UV-vis spectroscopy with the calibration curves of NF and DH standards at $\lambda_{max} = 384$ nm and $\lambda_{max} = 272$ nm, respectively. The experiment was repeated three times.

Drug loading of carrier (% wt)

$$= \frac{\text{amount of drug (mg)}}{\text{amount of materials and drug (mg)}} \times 100$$

In-vitro drug release studies were conducted using PBS pH 5.8 and pH 7.4. Five mg of drug-loaded materials were dissolved in 10 ml PBS at 37 °C while shaking at 150 rpm. At each time interval, 2 ml of the solution was centrifuged and replaced with fresh PBS of the same volume. The clear solution was pipetted through a nylon filter membrane after being centrifuged. The drug release concentration was determined using UV-vis spectrophotometry at 384 nm and 272 nm with the calibration curves of NF and DH standards. The cumulative release percentage was calculated as follows the equation:

$$\text{Drug release (\%)} = \frac{\text{amount of release drug}}{\text{amount of drug-loaded}} \times 100$$

Molecular modeling for explaining drug release behaviour

All molecular structures involved in the study were obtained from PubChem [19], except for ZIF-8 which was obtained from ChemTube3D [20] as a unit cell. Two polysaccharides, i.e., CS and BCD, each represented by a small fragment of its dimer. With the assistance of VESTA [21], the whole cage of ZIF-8 could be constructed. The initial structures of the molecular binding were carried out using the molecular docking technique (AutoDock4$_{Zn}$ software [22]). The best conformation of each interacting pair was generated using

a search method based on the Lamarckian genetic algorithm (LGA) in conjunction with a semiempirical free energy force-field [23], and a grid spacing were calculated using AutoGrid4 [24]. The best conformations generated by AutoDock4 were fed as inputs to obtain more accurate energies of binding (ΔE_{bind}) and structures based on density functional-based tight-binding (DFTB) calculations, which were performed with the DFTB+ package [25]. Structural analyses, such as H-bond formation and other favorable interactions, were performed with UCSF Chimera [26].

RESULTS AND DISCUSSION

Analysis of ZIF-8 and drug-encapsulated ZIF-8

The ZIF-8 is a drug delivery vehicle, and it is pH-sensitive. Several techniques were used to characterize the synthesized ZIF-8 and the drug encapsulated in ZIF-8. In this study, we compared the effects of drug loading methods using one-pot encapsulation (drug@ZIF-8) and drug-loaded ZIF-8. FE-SEM and TEM of the conventionally synthesized ZIF-8 DH and the NF encapsulation in ZIF-8 were shown in Fig. 1c-f. ZIF-8 particles had a rhombic dodecahedron shape and were 374 ± 24 nm in size [27]. The nanoparticle size of DH@ZIF-8 was measured at 118 ± 18 nm. The NF-loaded ZIF-8 and the NF@ZIF-8 had quite different shapes from each other, with sizes in the ranges of 537 ± 48 nm (Fig. 1d) and 207 ± 33 nm (Fig. 1f), respectively. This is because water is the solvent in one-pot synthesis, which could not grow to a 3D ZIF-8 network [28]. UV-visible, FT-IR, XRD, and TGA analyses of DH and NF encapsulation in ZIF-8 were depicted in Fig. 2a-f. The UV-vis spectra of drug loaded and one pot preparation were very similar, and the DH and NF drugs were incorporated into ZIF-8 (Fig. 2a,b). FT-IR observations showed that the ZIF-8 crystal had characteristic peaks at 3406, 3139 cm^{-1} (N−H) stretching, 1572, 1461, and 1420 cm^{-1} (C=N) stretching, 1142 and 994 cm^{-1} (C−N) stretching, 844 cm^{-1} (N−H) out-of-plane bending, and 421 cm^{-1} (Zn−N) stretching [17, 29]. The DH pure drug was presented at 2938 cm^{-1} (C−H) stretching, 2454 and 2421 cm^{-1} (N−H$^+$) stretching, 1588 cm^{-1} (C=O) stretching, 1498 cm^{-1} (C=C) stretching, 1215 cm^{-1} (C−O) stretching, 1115 and 1034 cm^{-1} (C−N) stretching, and 700 cm^{-1} (N−H) bending. The FT-IR spectra of drug-loaded ZIF-8 and one-pot synthesis were similar (see Fig. 2c,d). The DH@ZIF-8 spectrum contained ZIF-8 at 1456, 1422 cm^{-1} (C=N) and 1146, 996 cm^{-1} (C−N). The drug adsorbed DH showed at 1102 cm^{-1} (C−N). The bands of ZIF-8, C=N (1572 cm^{-1}) and DH, C=O (1588 cm^{-1}) were overlapping at the same peak at 1568 cm^{-1}.

NF showed peaks at 3281 cm^{-1} (N−H) stretching, at 3149 and 3110 cm^{-1} (C−H) stretching, at 1779 cm^{-1} and 1609 cm^{-1} for the (C=O) of imide in-phase, and out-of-phase, respectively. The asymmetric and symmetric stretching (N−O) of the nitro group (−NO$_2$) in NF was measured at 1562 cm^{-1} and 1379 cm^{-1}, respectively. The asymmetric and symmetric (C−O) bands of the furanyl group were observed at 1109 cm^{-1} and 926 cm^{-1}, respectively. NF@ZIF-8 contained ZIF-8 at 3132 cm^{-1} (N−H), at 2961 and 2924 cm^{-1} (C−H), at 1460 and 1421 cm^{-1} (C=N), at 1144 and 995 cm^{-1} (C−N), at 858 cm^{-1} (N−H) out-of-plane bending, and 422 cm^{-1} (Zn−N); and the asymmetric stretching of C=O, N−O and C−O from NF was observed at 1609, 1568 and 1032 cm^{-1}, respectively. XRD patterns of ZIF-8 exhibited reflection peaks at (011), (002), (112), (022), (013), and (222) [29, 30]. The XRD patterns of NF and NF-encapsulated ZIF-8 were shown in Fig. 2e. The characteristic peaks of NF at 14.48 as well as 16.60° were also found in the XRD patterns of NF-encapsulated ZIF-8.

The diffraction patterns of NF-loaded ZIF-8 and NF@ZIF-8 were nearly identical; however, in NF-loaded ZIF-8, a small unknown phase peak at 10.98° was obtained, which could indicate the presence of zinc phosphate impurity phases in the complex [31]. The TGA analysis of ZIF-8, DH@ZIF-8, and NF@ZIF-8 was shown in Fig. 2f. ZIF-8 was extremely thermally stable, with a decomposition temperature of around 450 °C [29]. NF@ZIF-8 exhibited weight loss of about 12% in the range of 220–400 °C, corresponding to the loss of NF molecules. At around 450–500 °C, the decomposition of ZIF-8 exhibited a sharp curve of weight loss. However, the TGA curve of DH@ZIF-8 did not show an obvious peak. It was assumed that DH might be trapped inside ZIF-8 pore, resulting in loss of DH and decomposition of ZIF-8 simultaneously.

Analysis of CS and BCD-incorporated ZIF-8 and drug encapsulation

SEM and TEM images of nanoparticle DH@ZIF-8/CS and NF@ZIF-8/CS were presented in Fig. 3. The surface of drug-encapsulated ZIF-8/CS becomes rougher and rounder as compared with the ZIF-8 surface. The average particle sizes for DH@ZIF-8/CS and NF@ZIF-8/CS were 117 ± 13 nm and 106 ± 12 nm, respectively. The drug-encapsulated ZIF-8/BCD, on the other hand, exhibited smooth surfaces, with a particle size of 118 ± 16 nm (DH@ZIF-8/BCD) and 114 ± 17 nm (NF@ZIF-8/BCD). Fig. 4a,b depicts the FT-IR spectra of CS and BCD-incorporated ZIF-8. The NF@ZIF-8/CS showed the character of CS coated NF@ZIF-8 at 1662 cm^{-1} (C=O imide I), at 1316 cm^{-1} (C−N amide III), at 1151 cm^{-1} (C−O saccharide), and at 1032 cm^{-1} (C−O−C glucosidic). On the other hand, the DH@ZIF-8/CS showed the CS bands at 1663, 1311, and 1021 cm^{-1} belonging to C=O, C−N, and C−O−C, respectively [32]. BCD showed the O−H stretching at 3320 cm^{-1}, the C−O−C stretching at 1153 cm^{-1}, and the C−O stretching with the OH group at 1080 and 1054 cm^{-1} [33]. We demonstrated peaks from
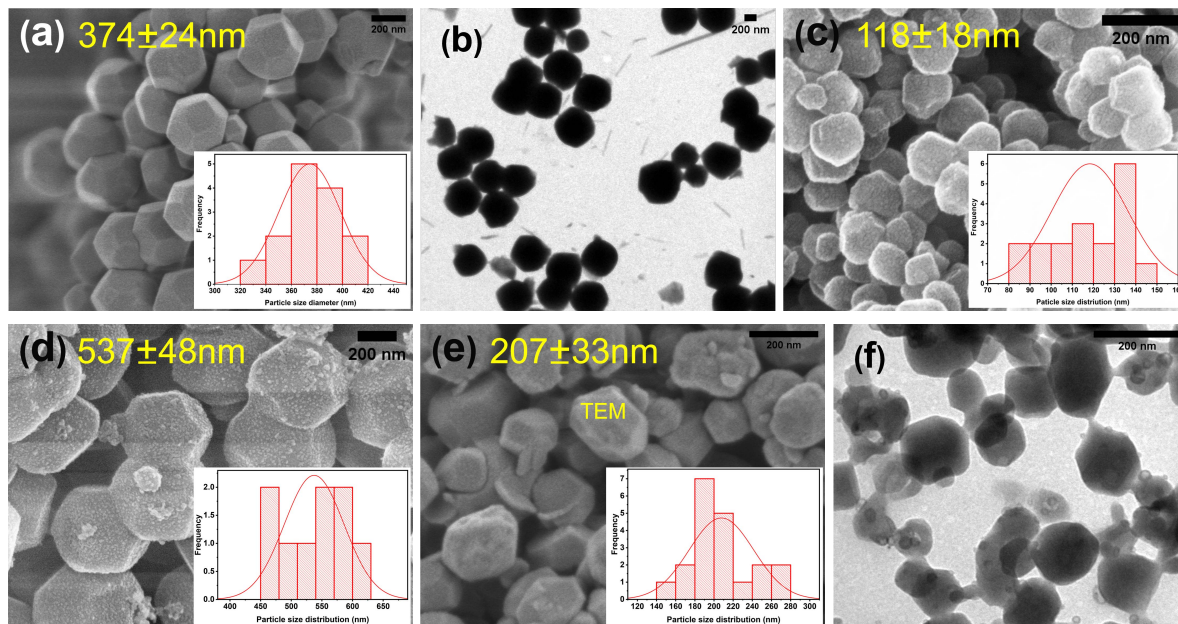
Fig. 1 (a), SEM image and particle size distribution histogram of ZIF-8; (b), TEM image of ZIF-8; (c), SEM image with particle size distribution histogram of DH@ZIF-8; (d), NF-loaded ZIF-8 with particle size distribution histogram; (e), NF@ZIF-8 with particle size distribution histogram; and (f), TEM image of NF-loaded ZIF-8.
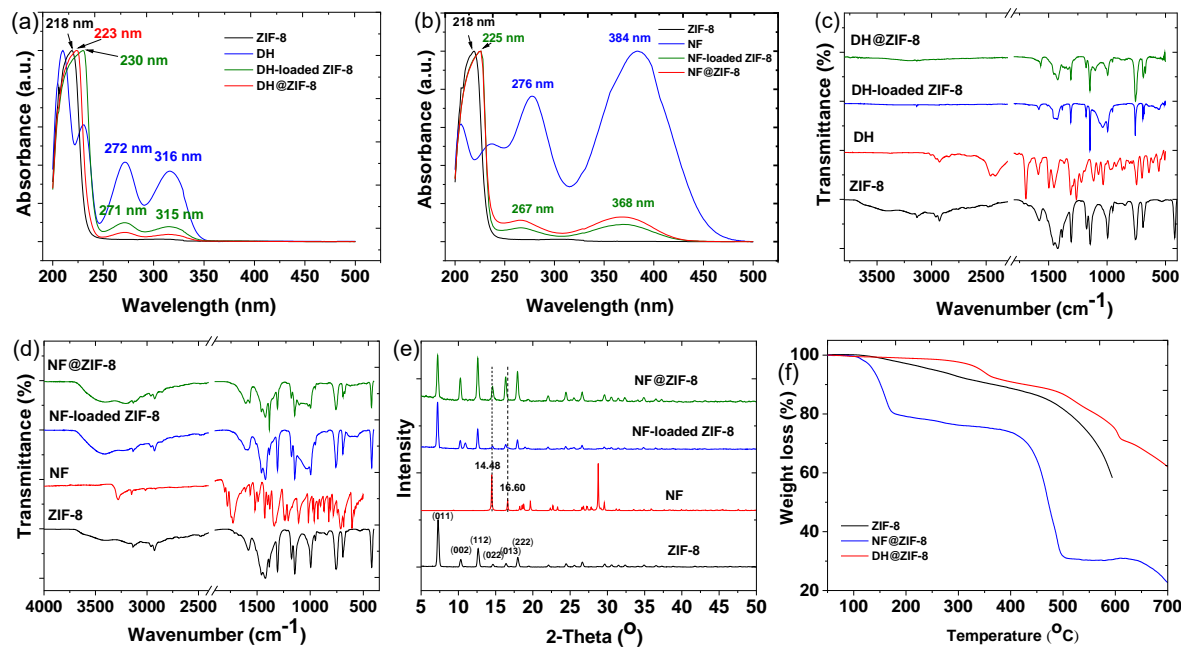

Fig. 2 UV-vis spectra of: (a), ZIF-8, DH, DH-loaded ZIF-8, and DH@ZIF-8; and (b), ZIF-8, NF, NF-loaded ZIF-8. FT-IR spectra of: (c), ZIF-8, DH, DH-loaded ZIF-8, and DH@ZIF-8; and (d), ZIF-8, NF, NF-loaded ZIF-8, and NF@ZIF-8; (e), XRD patterns of ZIF-8, NF, NF-loaded ZIF-8, and NF@ZIF-8; and (f), TGA thermogram of ZIF-8, DH@ZIF-8, and NF@ZIF-8.

BCD coated at 3313, 1149, 1083, and 1025 cm^{-1} for NF@ZIF-8/BCD; and the DH@ZIF-8/BCD showed weak bands at 3149, 1144, 1087, and 1040 cm^{-1} for O—H, C—O—C, and C—O with the OH group, respectively. As seen, the C=N at 1146 and 1144 cm^{-1} of ZIF-8 from NF@ZIF-8 and DH@ZIF-8 disappeared. XRD diffractions of drug-encapsulated ZIF-8/CS and ZIF-8/BCD were shown in Fig. 4c,d. As seen in
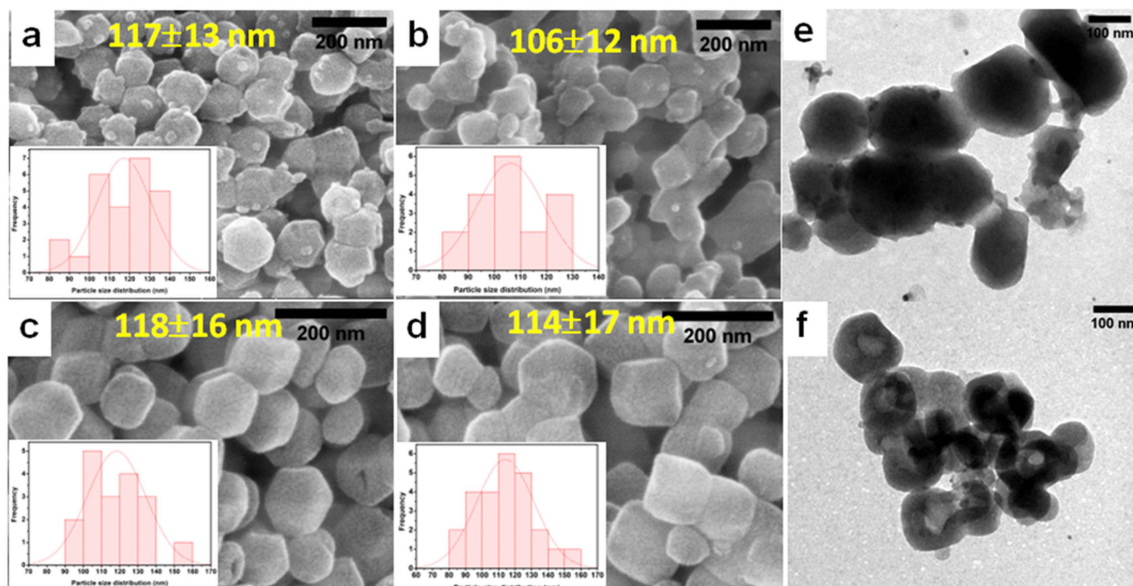
Fig. 3 SEM images and particle size distribution histograms of: (a), DH@ZIF-8/CS; (b), NF@ZIF-8/CS; (c), DH@ZIF-8/BCD; and (d), NF@ZIF-8/BCD; TEM images of: (e), DH@ZIF-8/CS; and (f), DH@ZIF-8/BCD.

Fig. 4c, the main diffraction peaks corresponded to ZIF-8 and the amorphous broad diffraction peak at 2θ about 10–25°; the two peaks at $2\theta = 10$ and 20° of CS [34] disappeared after being incorporated with drug-encapsulated ZIF-8. As a result of the chitosan, CS crystallization was reduced; and drug-encapsulated ZIF-8 was formed. The observation of ZIF-8/BCD was mainly that BCD covered ZIF-8 by obtaining the highlights from BCD peaks at 8.97 (101), 10.65 (130), 15.38 (141), and 19.53 (091) [35], and obtaining the overlap peaks of ZIF-8 and BCD from ZIF-8 at 12.66 (112), 17.97 (222), and 24.37° (114); and BCD at 12.48 (041), 17.92 (180), and 24.25° (162) (see Fig. 4d). The TGA and DTG curves of DH and NF-encapsulated ZIF-8 incorporating CS and BCD were shown in Fig. 4e,f. According to the thermogram, the first stage of thermal degradation of donepezil drug was observed between 87–88 °C [36]. The CS incorporated ZIF-8 showed a weight loss between 200–600 °C at 284 °C and 249 °C for DH@ZIF-8/CS and NF@ZIF-8/CS, respectively, corresponding to the process of organic linkage ligand degradation in ZIF-8 [37] and CS degradation [38] in the nanoparticles. Thermal breakdown of BCD-integrated ZIF-8 was observed in the temperature range of 200–450 °C, at 336 and 360 °C for DH@ZIF-8 and at 350 °C for NF@ZIF-8, correlating to ZIF-8 collapse and oligosaccharide fusion in BCD [39]. The zeta potential in the pH range of about 5 to 9 was used to evaluate the surface charge after modification of ZIF-8 with CS and BCD and the stability of drug delivery (see Fig. 4f,g). The zeta potential of DH@ZIF-8 was shown between +3.0 and −10.3 mV, with a positive charge below pH 6.2

and a negative charge at a higher pH. This behaviour could be attributed to hydrogen ions protonating and deprotonating nitrogen in the piperidine group. The NF@ZIF-8 showed a zeta potential of between −30.0 and +12.4 mV. It was found that the zeta potential was increased in both drugs after modifying the surface of ZIF-8 with CS and BCD. For CS modified-ZIF-8, DH was shown in the range of +15.8 to −37.0 mV, and NF was obtained in the range of +8.9 to −45.6 mV. The zero charges of DH and NF were at about pH 7.2 and 6.3, respectively. A positive charge at a lower pH and a negative charge at a higher pH were presented. This clearly confirmed the presence of CS on the modified surface of the ZIF-8; the zeta potential changes were due to the protonated amino group (the pKa of CS was 6.3). This result indicated that the CS-modified ZIF-8 surface was more stable at pH 7.4 for both drugs. However, the BCD-modified ZIF-8 obtained a negative charge over the range of −2.5 to −47.7 mV and −10.6 to −49.4 for DH and NF drugs, respectively.

Drug encapsulation and release

Eventually, we selected DH@ZIF-8 and NF@ZIF-8 for the study of drug release. The percentages of drug loading carrier were shown in Table S1. *In vitro* drug release behaviours of the DH and NF-encapsulated ZIF-8 and the CS and BCD-incorporated ZIF-8 were studied in PBS pH 5.8 and 7.4 simulations for 72 h, as shown in Fig. 5. The initial burst release of DH and NF at pH 5.8 at 6 h was approximately 83% and 75%, respectively; and a sustained release after 6 h with a maximum release of 92% and 77% in 72 h (see Fig. 5a,c). The cumulative releases of DH and NF were slower and
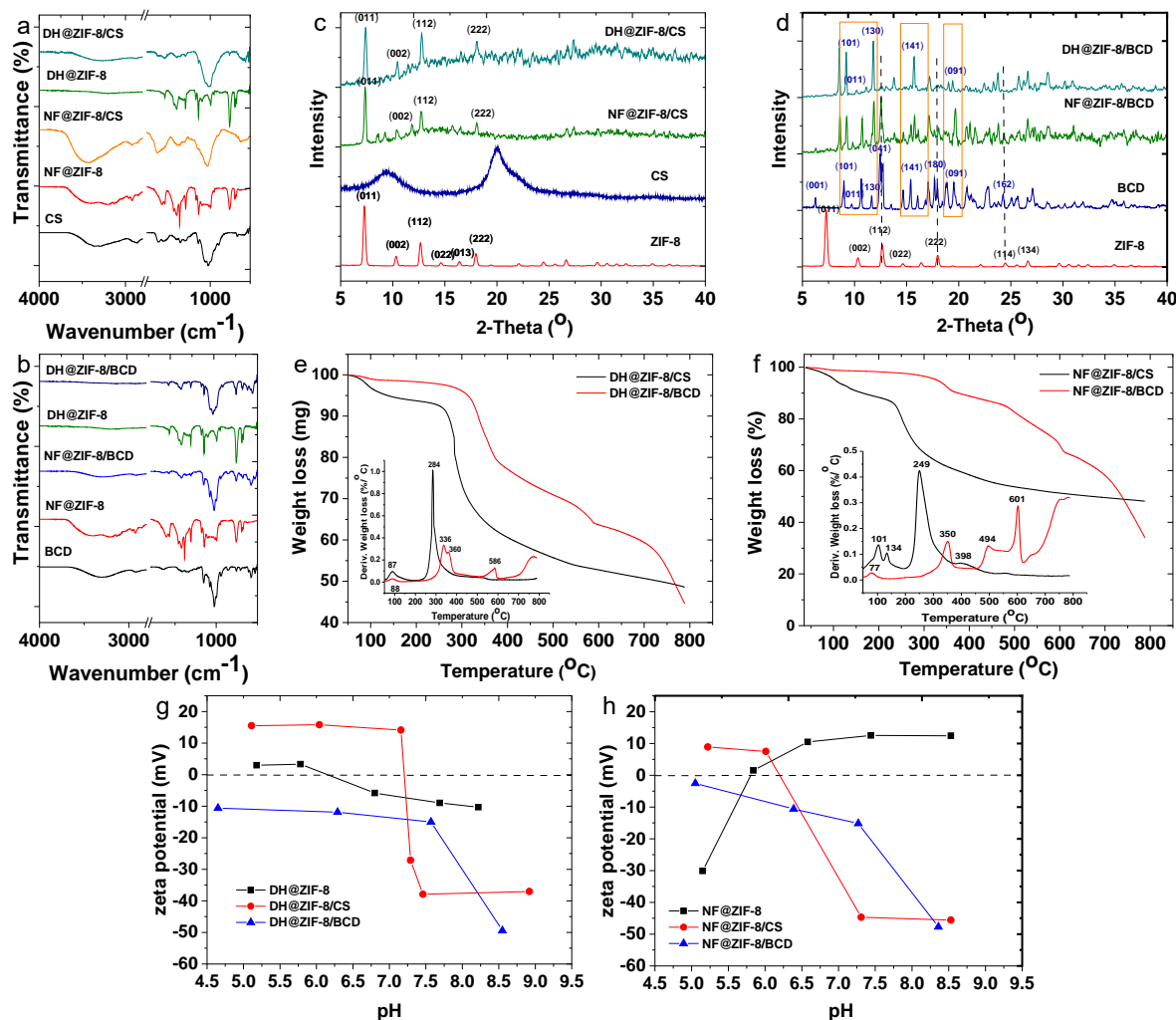
Fig. 4 FT-IR spectra of: (a), CS, NF@ZIF-8, NF@ZIF-8/CS, DH@ZIF-8, and DH@ZIF-8/CS; (b) BCD, NF@ZIF-8, NF@ZIF-8/BCD, DH@ZIF-8, and DH@ZIF-8/BCD; XRD patterns of: (c), ZIF-8, CS, NF@ZIF-8/CS, and DH@ZIF-8/CS; (d), ZIF-8, BCD, NF@ZIF-8/BCD, and DH@ZIF-8/BCD; (e), TGA and DTG thermograms of DH@ZIF-8/CS and DH@ZIF-8/BCD; and (f), TGA and DTG thermograms of NF@ZIF-8/CS and NF@ZIF-8/BCD; zeta potential at different pH values of: (g), DH@ZIF-8, DH@ZIF-8/CS and DH@ZIF-8/BCD; and (h), NF@ZIF-8, NF@ZIF-8/CS and NF@ZIF-8/BCD.

lower after the incorporation of the CS and the BCD with ZIF-8. The releases of DH and NF from DH@ZIF-8 and NF@ZIF-8 at pH 7.4 were slower and lower than at pH 5.8, with releasing percentages of 70% and 60% in the final 72 h, respectively (see Fig. 5b,d). The discussion would focus on computational details.

In vitro release kinetics and mechanisms were proposed by fitting with four mathematical models: zero-order, first-order, the Higuchi model, and the Koresmeyer-Peppas model [40]. Table S2 shows the coefficient (R^2) values from the fitting of the four mathematical models. From the equation fitting results, the correlation coefficient (R^2) showed that the Koresmeyer-Peppas was the best-fitting model (Fig. 5e,f) for pH 7.4. The mechanism of release was

indicated according to Korsmeyer-Peppas, where n was the release exponent, indicative of the mechanism of drug release. At pH 7.4, the R^2 of DH@ZIF-8 and the CS and BCD-incorporated ZIF-8 are higher than 0.9. The *n* values for DH@ZIF-8 and DH@ZIF-8/BCD were in the range of 0.45–0.89, which indicated a non-Fickian diffusion transfer. However, the *n* value for DH@ZIF-8/CS was smaller than 0.45, indicating that the drug release mechanism was Fickian diffusion-controlled. To confirm the release of drug from materials, SEM, FT-IR, and XRD techniques were employed, and the results were shown in Fig. S1. The hexagonal bipyramid was observed in SEM, and FT-IR demonstrated a new P—O stretching P—O stretching ($v_3(\text{PO}_4^{3-})$) and P—O bending ($v_4(\text{PO}_4^{3-})$) vibrational
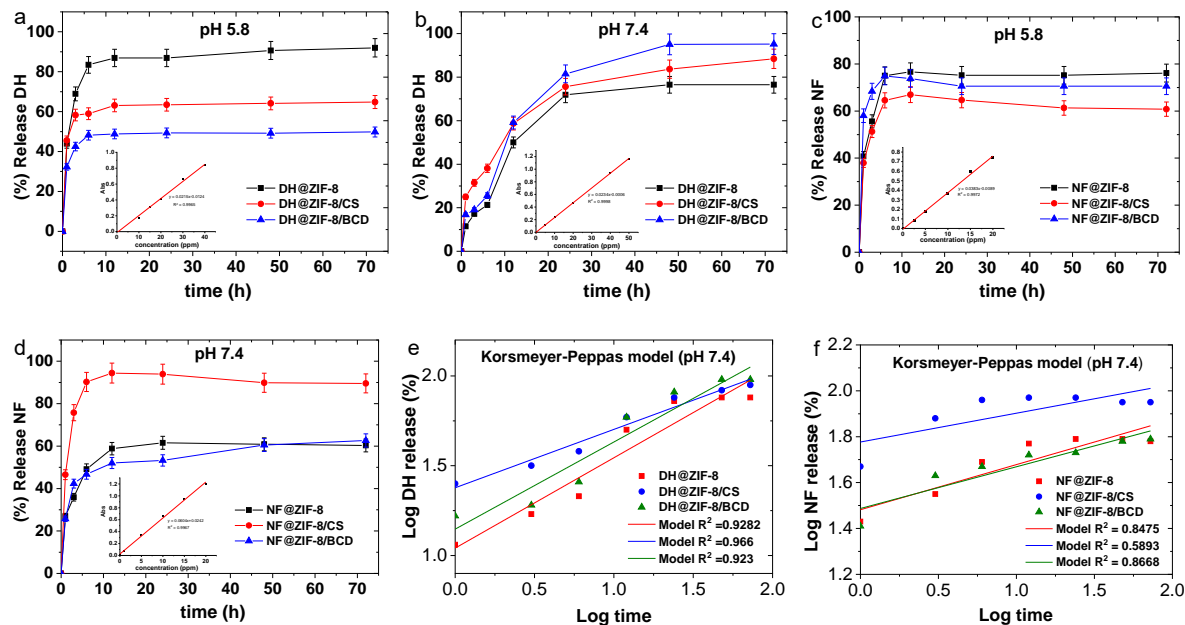
Fig. 5 *In vitro* release profiles of DH@ZIF-8, DH@ZIF-8/CS and DH@ZIF-8/BCD at: (a), pH 5.8; and (b), pH 7.4. *In vitro* release profiles of NF@ZIF-8, NF@ZIF-8/CS and NF@ZIF-8/BCD at: (c), pH 5.8; and (d), pH 7.4. Fitting of the drug delivery data to a Korsmeyer-Peppas model at pH 7.4: (e), DH; and (f), NF.

bands [41].

Molecular modeling for explaining the drug release behaviour

As seen in the experimental part, the XRD patterns of Drug@ZIF-8/CS and Drug@ZIF-8/BCD were like summations of the XRD patterns of ZIF-8 with CS, and BCD, respectively (Fig. 4c,d). This implied that 2-imidazole and Zn formed crystalline ZIF-8 as well as the incorporation of other components did not disturb the structure of ZIF-8. The SEM images (Fig. 1 and Fig. 3) could attest to the above interpretation because the shapes of individual multi-component materials were like sodalite cages, and no phase separation was observed. It was, therefore, assumed that ZIF-8 particles were core particles coated by other components. No other components other than Zn and 2-imidazole formed a covalent bond in ZIF-8. The material structure at the molecular level, which was deduced from the ΔE_{bind} and releasing behaviour of the material, was discussed in this section. The ΔE_{bind} between components was calculated and summarized in Table 1.

The ΔE_{bind} values of Pair No. 1 and Pair No. 3 were comparable, and the type of interaction between these two pairs was hydrophobic. This suggested that when ZIF-8 was forming, there was a chance that DH would be encapsulated as high as it covered the ZIF-8 surface. While the twice lower ΔE_{bind} of Pair No. 2 compared with that of Pair No. 4 indicated that NF preferred binding and formed a coordinate bond to

Zn. The calculations of Pairs No. 6–8 indicated that high energy barriers did not allow both DH and NF to penetrate from the surface to the interior of the cage. Since DH and NF contributed to ZIF-8 differently, it should be noted that the difference could also happen in the coating layer. To avoid confusion, discussion, the release of drugs based on molecular modeling was discussed individually.

For DH, at pH 7.4, the order of drug release was DH@ZIF-8/BCD > DH@ZIF-8/CS > DH@ZIF-8. As it was mentioned earlier, DH was bound to the pore as well as the surface. Hydrophobic interaction implied a less specific orientation in binding because of high drug loading on ZIF-8. The drug release of DH@ZIF-8 was the lowest because the strongest interaction was presented by the direct adsorption of DH on the ZIF-8 surface (Pair No. 1). While the ZIF-8 surface of the other two materials contributed to coating materials, it caused some of the DH to be bound to coating materials with weaker interaction (Pairs No. 11, 13). As a result, higher drug release was observed on DH@ZIF-8/BCD and DH@ZIF-8/CS. The difference in drug release between DH@ZIF-8/BCD and DH@ZIF-8/CS could be further explained via physical properties such as solubility and viscosity. The ΔE_{bind} values of Pairs No. 10 and 13 were comparable to Pairs No. 9 and 11, respectively. The drug release of DH@ZIF-8/CS was relatively lower than that of DH@ZIF-8/BCD because the entanglement of open-chain macromolecular CS made the medium more viscous and delayed the DH release.

Table 1 Component pairs, their energies of binding (ΔE_{bind}) and type of binding interaction.[†]

Pair no.	Component pair	ΔE_{bind} (kcal/mol)	Binding interaction
1	ZIF-8 (surface) – DH	–53.05	hydrophobic
2	ZIF-8 (surface) – NF	–86.78	Zn-N Coordinate bond (methylidene amino group of NF – Zn of ZIF-8)
3	ZIF-8 (cage) – DH	–58.98	hydrophobic
4	ZIF-8 (cage) – NF	–44.33	hydrophobic
5	ZIF-8(window) – DH (methoxy group)	+24.52	hydrophobic
6	ZIF-8 (window) – DH (benzene ring)	–5.06	hydrophobic
7	ZIF-8 (window) – NF (nitrofuran group)[‡]	–81.82	hydrophobic
8	ZIF-8 (window) – NF (imide group)	–12.12	hydrophobic
9	ZIF-8 (surface) – BCD	–46.43	hydrophobic
10	ZIF-8 (surface) – CS	–47.60	hydrophobic
11	BCD – DH	–23.86	H-bond 2nd hydroxyl of BCD(D) – methoxy of DH (A)
12	BCD – NF	–17.15	H-bond 2nd hydroxyl group of BCD (D) – nitrogroup of NF (A)
13	CS – DH	–21.18	H-bond 2nd hydroxyl group of CS (D) – carbonyl group of DH (A)
14	CS – NF	–19.09	3 H-bonds 2nd hydroxyl (D) – nitro (A) Amine (D – nitro (A) Amine (D) – methylidene amino (A)
15	ZIF-8 (surface) – DH(NH$^+$)	–12.75	Hydrophobic
16	CS(NH$_3^+$) – DH	–53.56	2 H-bond Amine (D) – carbonyl (A) Amine (D) – methoxy (A)
17	BCD – DH(NH$^+$)	–33.69	H-bond 2nd hydroxy (A) – amine (D)
18	CS – DH(NH$^+$)	–41.06	H-bond Pyranose O (A) – amine (D)
19	CS(NH$_3^+$) – DH(NH$^+$)	25.10	H-bond Amine (D) – carbonyl (A)
20	CS(NH$_3^+$) – NF	–41.46	2 H-bond Amine (D) – nitro (A) Amine (D) – carbonyl (A)

[†] H-bonds were considered using atom types and geometric criteria [42].

[‡] After geometric optimization, NF moved out of the ZIF-8 window and bound to the surface.

The drug release behaviour changed at pH 5.8. The higher release of DH@ZIF-8 was a result of ZIF-8 crumpling in an acidic condition. The coating material helped the drug release of DH@ZIF-8/BCD and DH@ZIF-8/CS become lower. However, the higher drug release of DH@ZIF-8/CS than that of DH@ZIF-8/BCD was assumed to involve a greater number of protonated amine groups in both CS and DH at lower pH. In the case of DH@ZIF-8/BCD, the amine group was present in DH only, and the ΔE_{bind} values of Pairs No. 13 and 16 indicated that the amino group could bind to BCD with stronger interaction when the amine group was protonated. The situation was more delicate when the coating layer was CS since the amine group could be present in both DH and CS. If either CS or DH was protonated (Pair No. 16 or 18), the attraction became stronger and caused lower DH release. But if both CS and DH, which interacted with each other, were protonated, the repulsion occurred (Pair No. 19). Therefore, the overall situation was lower in drug release for DH@ZIF-8/CS, but it was not lower than drug release for DH@ZIF-8/BCD, on which only stronger interactions could happen.

For the NF, the N-Zn coordinate bond limited the

NF bound to the surface of ZIF-8. A multilayer of adsorbed hydrophobic NF could be formed and cause slow drug release. Even though multilayers of NF could be formed, lots of NF as free molecules could exist in one-pot synthesis. The free voids of the coating CS were assumed to play the role of NF storage for NF@ZIF-8/CS. At pH 7.4, therefore, among three materials (Fig. 5d), the NF release of NF@ZIF-8/CS was the highest because NF was released as soon as CS permeated an aqueous medium. Similar NF release behaviours could be observed for NF@ZIF-8 and NF@ZIF-8/BCD. It was assumed that BCD, which was water-soluble, detached rapidly, and then ZIF-8/BCD became more like ZIF-8. In an acidic environment (Fig. 5c), the NF release behaviour of NF@ZIF-8/CS could be explained in a similar way to DH@ZIF-8/CS, i.e., the amine group that was protonated (ΔE_{bind} of Pair No. 20 < Pair No. 14). Since the acidic condition did not change the functional group of BCD, the NF release behaviour of NF@ZIF-8/BCD at pH 5.8 was much like that at pH 7.4, i.e., BCD was detached and followed by NF release. A slightly higher NF release of NF@ZIF-8 than NF@ZIF-8/BCD was observed because of direct contact with an acidic medium with no protection.

CONCLUSION

Encapsulations into ZIF-8 of DH (DH@ZIF-8) and NF (NF@ZIF-8) *via* one-pot synthesis were successful. Two types of saccharides, CS and BCD, were introduced as coating materials and developed as new drug carriers; namely, drug@ZIF-8/CS and drug@ZIF-8/BCD, respectively. It was found that changes in drug release behaviours did not depend only on the coating material but also on the loaded drugs (DH or NF). With the assistance of molecular modelling, the qualitative picture of drug release behaviours became clearer. In the case of DH, the drug preferred adsorption in the interior and on the surface of ZIF-8. It was found that at an acidic pH, protonation of the amine groups of CS and DH caused stronger ΔE_{bind} and could play a role in slower drug release. In the case of NF, in addition to preferential adsorption on the surface of ZIF-8, the drug also formed an N-Zn coordinate bond, which resulted in limiting loading. The free voids of CS played the role of storage for NF and caused higher loading. Acidic conditions caused slower drug release for NF@ZIF-8/CS, and the same assumption was proposed for DH@ZIF-8/CS. The results reported here could be useful as guidelines for developing drug-loaded carriers based on metal-organic frameworks and biopolymers.

Appendix A. Supplementary data

Supplementary data associated with this article can be found at http://dx.doi.org/10.2306/scienceasia1513-1874.2023.078.

REFERENCES

1. Ahuja G, Pathak K (2009) Porous carriers for controlled/modulated drug delivery. *Indian J Pharm Sci* **71**, 599–607.
2. Feng S, Zhang X, Shi D, Wang Z (2021) Zeolitic imidazolate framework-8 (ZIF-8) for drug delivery: a critical review. *Front Chem Sci Eng* **15**, 221–237.
3. Tran VA, Lee S-W (2021) pH-triggered degradation and release of doxorubicin from zeolitic imidazolate framework-8 (ZIF8) decorated with polyacrylic acid. *RSC Adv* **11**, 9222–9234.
4. Wu Q, Niu M, Chen X, Tan L, Fu C, Ren X, Ren J, Li L, et al (2018) Biocompatible and biodegradable zeolitic imidazolate framework/polydopamine nanocarriers for dual stimulus triggered tumor thermo-chemotherapy. *Biomater* **162**, 132–143.
5. Miao T, Wang J, Zeng Y, Liu G, Chen X (2018) Polysaccharide-based controlled release systems for therapeutics delivery and tissue engineering: from bench to bedside. *Adv Sci* **5**, 1700513.
6. Li Y, Zheng Y, Lai X, Chu Y, Chen Y (2018) Biocompatible surface modification of nano-scale zeolitic imidazolate frameworks for enhanced drug delivery. *RSC Adv* **8**, 23623–23628.
7. Vahed TA, Naimi-Jamal MR, Panahi L (2019) Alginate-coated ZIF-8 metal-organic framework as a green and bioactive platform for controlled drug release. *J Drug Deliv Sci Technol* **49**, 570–576.
8. Singh A, Mittal A, Benjakul S (2021) Chitosan nanoparticles: preparation, food applications and health benefits. *ScienceAsia* **47**, 1–10.
9. Hidalgo T, Giménez-Marqués M, Bellido E, Avila J, Asensio MC, Salles F, Lozano MV, Guillevic M, et al (2017) Chitosan-coated mesoporous MIL-100(Fe) nanoparticles as improved bio-compatible oral nanocarriers. *Sci Rep* **7**, 43099.
10. Maheriya PM (2017) Cyclodextrin: A promising candidate in enhancing oral bioavailability of poorly water soluble drugs. *MOJ Bioequiv Availab* **3**, 60–63.
11. Viernstein H, Wolschann P (2020) Cyclodextrin inclusion complexation and pharmaceutical applications. *ScienceAsia* **46**, 254–262.
12. Agostoni V, Horcajada P, Noiray M, Malanga M, Aykaç A, Jicsinszky L, Vargas-Berenguel A, Semiramoth N, et al (2015) A "green" strategy to construct non-covalent, stable and bioactive coatings on porous MOF nanoparticles. *Sci Rep* **5**, 7925.
13. Vangala VR, Chow PS, Tan RBH (2012) Co-crystals and co-crystal hydrates of the antibiotic nitrofurantoin: structural studies and physicochemical properties. *Cryst Growth Des* **12**, 5925–5938.
14. Sugimoto H, Ogura H, Arai Y, Iimura Y, Yamanishi Y (2002) Research and development of donepezil hydrochloride, a new type of acetylcholinesterase inhibitor. *Jpn J Pharmacol* **89**, 7–20.
15. Aderibigbe BA, Naki T (2019) Chitosan-based nanocarriers for nose to brain delivery. *Appl Sci* **9**, 2219.
16. Amjad MW, Alotaibi NM (2020) Formulation and in vitro characterization of donepezil-loaded chitosan nanoparticles. *J Pharm Res Int* **32**, 10–16.
17. Liu T, Wan X, Luo Z, Liu C, Quan P, Cun D, Fang L (2019) A donepezil/cyclodextrin complexation orodispersible film: effect of cyclodextrin on taste-masking based on dynamic process and *in vivo* drug absorption. *Asian J Pharm Sci* **14**, 183–192.
18. Adhikari C, Das A, Chakraborty A (2015) Zeolitic imidazole framework (ZIF) nanospheres for easy encapsulation and controlled release of an anticancer drug doxorubicin under different external stimuli: a way toward smart drug delivery system. *Mol Pharm* **12**, 3158–3166.
19. Kim S, Chen J, Cheng T, Gindulyte A, He J, He S, Li Q, Shoemaker BA, et al (2021) PubChem in 2021: new data content and improved web interfaces. *Nucleic Acids Res* **49**, D1388–D1395.
20. Hanwell MD, Curtis DE, Lonie DC, Vandermeersch T, Zurek E, Hutchison GR (2012) Avogadro: An advanced semantic chemical editor, visualization, and analysis platform. *J Cheminform* **4**, 17.
21. Momma K, Izumi F (2011) VESTA 3 for three-

dimensional visualization of crystal, volumetric and morphology data. *J Appl Crystallogr* **44**, 1272–1276.

22. Morris GM, Huey R, Lindstrom W, Sanner MF, Belew RK, Goodsell DS, Olson AJ (2009) Autodock4 and AutoDock-Tools4: automated docking with selective receptor flexiblity. *J Comput Chem* **16**, 2785–2791.

23. Huey R, Morris GM, Olson AJ, Goodsell DS (2007) A semiempirical free energy force field with charge-based desolvation. *J Comput Chem* **28**, 1145–1152.

24. Goodford PJ (1985) A computational procedure for determining energetically favorable binding sites on biologically important macromolecules. *J Med Chem* **28**, 849–857.

25. Hourahine B, Aradi B, Blum V, Bonafé F, Buccheri A, Camacho C, Cevallos C, Deshaye MY, et al (2020) DFTB+, a software package for efficient approximate density functional theory based atomistic simulations. *J Chem Phys* **152**, 124101.

26. Pettersen EF, Goddard TD, Huang CC, Couch GS, Greenblatt DM, Meng EC, Ferrin TE (2004) UCSF Chimera-a visualization system for exploratory research and analysis. *J Comput Chem* **25**, 1605–1612.

27. Schejn A, Balan L, Falk V, Aranda L, Medjahdic G, Schneider R (2014) Controlling ZIF-8 nano- and microcrystal formation and reactivity through zinc salt variations. *Cryst Eng Comm* **16**, 4493–4500.

28. Tezerjani AA, Halladj R, Askari S (2021) Different view of solvent effect on the synthesis methods of zeolitic imidazolate framework-8 to tuning the crystal structure and properties. *RSC Adv* **11**, 19914–19923.

29. Kaur H, Mohanta GC, Gupta V, Kukkar D, Tyagi S (2017) Synthesis and characterization of ZIF-8 nanoparticles for controlled release of 6-mercaptopurine drug. *J Drug Deliv Sci Technol* **41**, 106–112.

30. Nordin NAHM, Ismail AF, Yahya N (2017) Zeolitic imidazole framework 8 decorated graphene oxide (ZIF-8/GO) mixed matrix membrane (MMM) for CO_2/CH_4 separation. *J Teknol (Sci Eng)* **79**, 59–63.

31. Chennah A, Naciri Y, Taoufyq A, Bakiz B, Bazzi L, Guinneton F, Villain S, Gavarri JR, et al (2019) Electrodeposited zinc phosphate hydrate electrodes for electrocat-

alytic applications. *J Appl Electrochem* **49**, 163–177.

32. Govindan S, Nivethaa EAK, Saravanan R, Narayanan V, Stephen A (2012) Synthesis and characterization of chitosan-silver nanocomposite. *Appl Nanosci* **2**, 299–303.

33. Roik NV, Belyakova LA (2011) Thermodynamic, IR spectral and X-ray diffraction studies of the "β-cyclodextrin-para-aminobenzoic acid" inclusion complex. *J Incl Phenom Macrocycl Chem* **69**, 315–319.

34. Wang X, Du Y, Liu H (2004) Preparation, characterization and antimicrobial activity of chitosan-Zn complex. *Carbohydr Polym* **56**, 21–26.

35. Song W, Yu X, Wang S, Blasier R, Markel DC, Mao G, Shi T, Ren W (2011) Cyclodextrin-erythromycin complexes as a drug delivery device for orthopedic application. *Int J Nanomed* **6**, 3173–3186.

36. Guo W, Quan P, Fang L, Cun D, Yang M (2015) Sustained release donepezil loaded PLGA microspheres for injection: Preparation, *in vitro* and *in vivo* study. *Asian J Pharm Sci* **10**, 405–414.

37. Tran UPN, Le KKA, Phan NTS (2011) Expanding applications of metal-organic frameworks: zeolite imidazolate framework ZIF-8 as an efficient heterogeneous catalyst for the Knoevenagel reaction. *ACS Catal* **1**, 120–127.

38. Ziegler-Borowska M, Chelminiak D, Kaczmarek H (2015) Thermal stability of magnetic nanoparticles coated by blends of modified chitosan and poly(quaternary ammonium) salt. *J Therm Anal Calorim* **119**, 499–506.

39. Sambasevam KP, Mohamad S, Sarih NM, Ismail NA (2013) Synthesis and characterization of inclusion complex of β-cyclodextrin and azomethine. *Int J Mol Sci* **14**, 3671–3682.

40. Dash S, Murthy PN, Nath L, Chowdhury P (2010) Kinetic modelling on drug release from controlled drug delivery system. *Acta Pol Pharm* **67**, 217–223.

41. Velásquez-Hernández MJ, Ricco R, Carraro F, Limpoco FT, Linares-Moreau M, Leitner E, Wiltsche H, Rattenberger J, et al (2019) Degradation of ZIF-8 in phosphate buffered saline media. *Cryst Eng Comm* **21**, 4538–4544.

42. Mills JE, Dean PM (1996) Three-dimensional hydrogen-bond geometry and probability information from a crystal survey. *J Comput Aided Mol Des* **10**, 607–622.
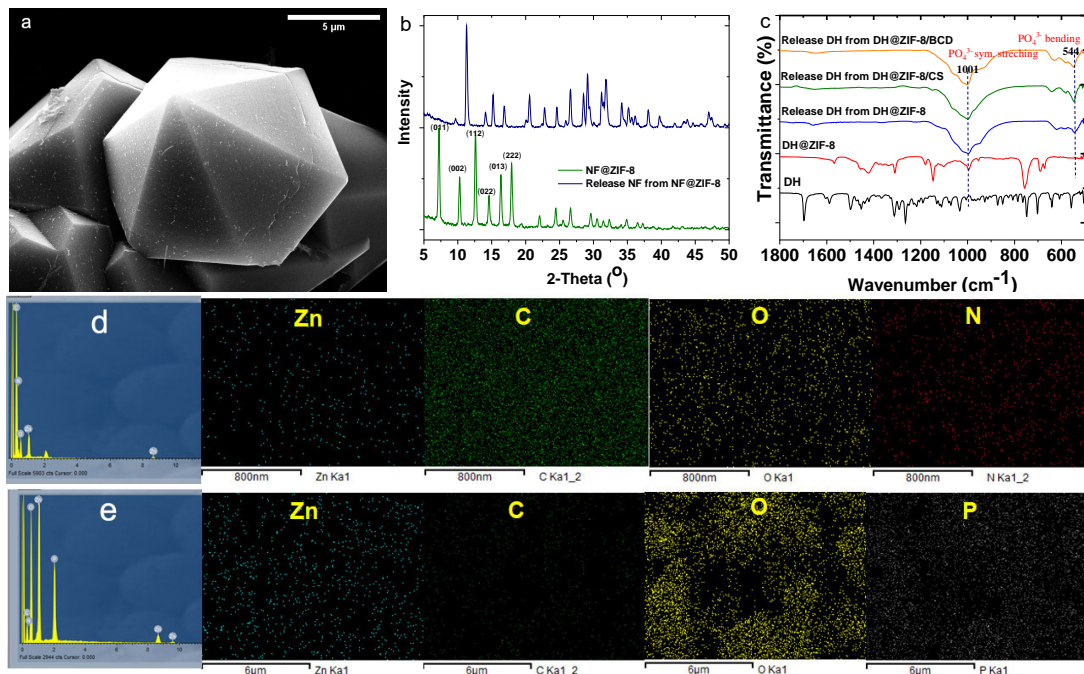
Appendix A. Supplementary data

Fig. S1 (a), SEM image of DH@ZIF-8/CS; (b), XRD pattern of NF@ZIF-8 and NF-released from NF@ZIF-8; (c), FT-IR spectra of DH and DH-released from DH@ZIF-8, DH@ZIF-8/CS and DH@ZIF-8/BCD; (d), EDS spectrum of NF@ZIF-8 and element mapping of Zn, C, O, N; and (e), EDS spectrum of NF-released from NF@ZIF-8 and element mapping of Zn, C, O, N, NF and NF-released from NF@ZIF-8.

Table S1 Drug loading of carrier (% wt) in ZIF-8, ZIF-8/CS and ZIF-8/BCD.

Sample	Loading of target molecule (%wt)	Sample	Loading of target molecule (%wt)
DH@ZIF-8	2.58 ± 0.065	NF@ZIF-8	0.96 ± 0.05
DH@ZIF-8/CS	1.79 ± 0.018	NF@ZIF-8/CS	1.73 ± 0.61
DH@ZIF-8/BCD	2.46 ± 0.073	NF@ZIF-8/BCD	0.36 ± 0.03

Table S2 Kinetics model fitting results of drug release data.

pH	Sample	Mathematic model/Equation				
		Zero order	First order	Higuchi	Koresmeyer-Peppas	
		$Q_t = Q_0 + k_0 t$	$\log Q_t = \log Q_0 - k_1 t / 2.303$	$Q_t = K_H t^{1/2}$	$Q_t = K_{kp} t^n$	
		R^2	R^2	R^2	R^2	n
5.8	DH@ZIF-8	0.3962	0.3286	0.5685	0.7509	0.15
	DH@ZIF-8/CS	0.3904	0.3492	0.5593	0.7517	0.07
	DH@ZIF-8/BCD	0.3088	0.2972	0.4755	0.7161	0.09
	NF@ZIF-8	0.2890	0.2849	0.4562	0.7187	0.13
	NF@ZIF-8/CS	0.1278	0.1321	0.2667	0.5408	0.10
	NF@ZIF-8/BCD	0.0577	0.0942	0.1436	0.4386	0.04
7.4	DH@ZIF-8	0.7132	0.6157	0.8610	0.9282	0.50
	DH@ZIF-8/CS	0.7944	0.7030	0.9252	0.9660	0.33
	DH@ZIF-8/BCD	0.7687	0.6692	0.8980	0.9230	0.49
	NF@ZIF-8	0.4429	0.4101	0.6397	0.8475	0.20
	NF @ZIF-8/CS	0.1887	0.1780	0.3430	0.5893	0.13
	NF @ZIF-8/BCD	0.6421	0.4882	0.7952	0.8668	0.18